A Novel Growth Mode of Mo on Au (111) from a $Mo(CO)_6$ Precursor: An STM Study

Zhen Song,[†] Tanhong Cai,[†] Jose A. Rodriguez,[†] Jan Hrbek,*[,†] Ally S. Y. Chan,[‡] and Cynthia M. Friend[‡]

Chemistry Department, Brookhaven National Laboratory, Upton, New York 11973, and Department of Chemistry and Division of Engineering and Applied Sciences, Harvard University, 12 Oxford Street, Cambridge, Massachusetts 02138

Received: September 20, 2002; In Final Form: December 4, 2002

The growth of a submonolayer of metallic Mo prepared by chemical vapor deposition (CVD) of $Mo(CO)_6$ on Au(111) was studied by scanning tunneling microscopy (STM). At low coverage, nanoscale Mo clusters grow at the elbow sites and in the fcc regions of the reconstructed Au surface. When the coverage increases, rather than decorating uniformly all elbows as found in physical vapor deposition (PVD), the Mo clusters aggregate but do not coalesce, forming ramified cluster islands. Within the islands, the clusters preferentially aggregate along the fcc troughs and the domain boundaries. At step edges, Mo clusters are found to grow at both upper and lower step edges. Differences between CVD and PVD are attributed to differences in the mobility of the nascent Mo species leading to growth. We hypothesize that the difference in mobility for the CVD process is due to the presence of CO from the precursor molecules. Oxidation of the Mo islands leads to their spreading, proving that the Mo clusters are either three-dimensional above or embedded in the surface of the gold substrate.

Introduction

Use of metal carbonyls in chemical vapor deposition (CVD) has been attractive for both the synthesis of supported metal catalysts and the fabrication of electronic devices. In catalyst manufacturing, CVD using metal carbonyls has clear advantages in preparation of zerovalent metal clusters of very small size and high dispersion.[1−3] Catalysts made this way show improved performance such as higher selectivity or activity.[4−9] Furthermore, metal carbonyls provide flexibility in terms of catalyst composition since they are readily available for a broad range of metals. Advantages of CVD of metals on semiconductors in electronics applications are selectivity, conformal step coverage, high throughput, and low cost.[10] Many studies have focused on finding the decomposition conditions of metal carbonyls for obtaining naked metals and also on the structure and reactivity of the deposited metal clusters or films.[11,12] Recently, Argo et al.[13] showed that the metal framework structure of certain multinuclear metal carbonyls, e.g., $Ir_4(CO)_{12}$, stays intact after decarbonylation in inert atmosphere at elevated temperatures. The use of this approach may allow the preparation of naked metal clusters with the preserved original metal skeleton of the carbonyls.

Molybdenum hexacarbonyl ($Mo(CO)_6$) interacts with metal surfaces at low temperatures forming physisorbed layers of the molecular carbonyl.[11,12,14] Upon heating, most condensed carbonyl molecules sublime without decomposition with an activation energy about 14 kcal/mol and only a small fraction of the first carbonyl layer dissociates on the Au substrate.[15] Since the gas-phase dissociation energy for cleavage of the first CO−$Mo(CO)_5$ bond is about 40 kcal/mol,[16] thermal activation is needed for an efficient decomposition of the carbonyl on noble metal surfaces. The ratio of decomposition to desorption is higher on metal surfaces that bind CO strongly, e.g., Ni,[12] because this provides an additional thermodynamic driving force for dissociation of the metal−CO bond. One limitation of metal CVD using metal carbonyls is that CO released during the deposition process may lead to incorporation of carbon and oxygen impurities in the growing metal layer. Therefore, optimization of the deposition conditions is critical for growth of a clean metal layer.

We have recently prepared Mo particles on Au(111) by $Mo(CO)_6$ CVD and studied their reactivity using synchrotron-based photoemission spectroscopy (PES).[15] The selection of Mo on Au(111) is based on the idea of using a patterned substrate for preparation of a model catalyst with well-defined structural and size distributions that will allow the study of the relationship between nanoscale structures and reactivity. Mo-based catalysts are widely used in the petroleum and chemical industries for olefin metathesis, alkene hydrogenation, isomerization, and hydrotreatment of oil-derived feedstock (hydrodesulfurization, hydrodenitridation, hydrodeoxidation).[17−20]

The reconstructed Au(111)−$(22 \times \sqrt{3})$ surface was chosen as a support due to its chemical inertness and its dislocation network that can be used as a template for growing self-organized cluster arrays.[21−31] In principle, the preparation of well-ordered arrays of monodispersed, nanometer-scale clusters can be accomplished by using patterned substrates formed spontaneously in heteroepitaxial systems or at reconstructed surfaces.[32,33] Strain relief in such surfaces causes formation of periodic dislocation networks that are often ordered into regular arrays. The herringbone reconstruction of the Au(111) surface is one of the best known examples of the dislocation networks.[21] The reconstruction is driven by the tensile stress in the top Au layer and partial dislocation stripes form to separate alternating fcc and hcp stacking regions. The surface, uniaxially contracted along {110} directions, forms a superstructure with stress

* Corresponding author. E-mail: hrbek@bnl.gov.
[†] Brookhaven National Laboratory.
[‡] Harvard University.

10.1021/jp0270405 CCC: $25.00
Published on Web 01/07/2003

domains alternating in a zigzag pattern. The dislocation stripes meet at the domain boundaries to form edge dislocations, the elbows. The binding energies and energy barriers for surface diffusion of deposited adatoms may, therefore, be periodically modulated, and, thus, may modify nucleation and growth processes.

Previous studies of metal deposition on reconstructed Au(111) have demonstrated that it is an excellent template for self-organized growth of metal nanostructures. Several different nucleation and growth modes have been observed for metal growth using physical vapor deposition (PVD) on the Au(111) herringbone. Preferential nucleation of metal clusters at elbows of the herringbone reconstruction have been observed for transition metals that have a higher surface free energy than Au, such as Ni,[22] Fe,[23] Co,[24−26] Rh,[27] and Mo.[28] High nucleation probability at elbows was originally explained by the trapping of Ni adatoms at attractive potential wells present at the elbow sites.[22] Recently, site-selective place exchange of Ni adatoms and surface Au atoms, followed by preferential nucleation at the exchange sites, has been proposed to explain the nucleation at the elbows. On the other hand, noble metals, e.g., Au[29] and Ag,[30,31] grow from the Au step edges into the fcc region to form fingerlike rows. In contrast, Al clusters were found to nucleate only between dislocation lines in the fcc areas of the Au reconstruction implying a strong repulsion of adatoms at dislocations.[34,35] Similarly, electrochemically deposited Ru clusters also nucleate selectively in the fcc regions of the herringbone and grow there to form nanowires confined to the fcc domains.[36]

We are interested in using CVD methods to grow organized nanostructures on reconstructed Au(111). Herein, we present STM results for the CVD of Mo on Au(111) using $Mo(CO)_6$ as a precursor. We find that Mo nanoclusters grow at elbows and fcc areas, and that these clusters aggregate to form ramified islands along fcc troughs and domain boundary directions of the Au(111)−$(22\times\sqrt{3})$ reconstruction. The data reveal a novel growth mode of Mo on the reconstructed gold in which Mo clusters aggregate without coalescence. This finding is a sharp contrast to the type of growth observed for PVD of Mo on Au(111) recently.[28] The large mobility of the Mo clusters with remnant or re-adsorbed CO ligands is the major reason for the observed morphology.

Experiment

The experiments were performed in two separate UHV chambers, both of which were equipped with a scanning tunneling microsope (STM), sputter gun, and LEED/Auger for sample characterization. In the chamber at Brookhaven, an Omicron STM was used to obtain images and a preparation chamber was configured for sample cleaning, annealing, and preparation using a chemical vapor deposition doser. The Au(111) surface was cleaned by cycles of Ne^+ sputtering (600 eV, 2 μA) at room temperature followed by 900 K annealing. The Au samples were deemed clean when STM images exhibited extended domains of periodic herringbone reconstruction. At Harvard, a beetle-type STM was used, which has been described elsewhere.[37] The Au sample was cleaned by cycles of Ar^+ bombardment (1 keV, 3 μA) and annealing to 900 K. The surface was determined to be clean by Auger electron spectroscopy and the observation of the herringbone reconstruction using both LEED and STM.

Molybdenum deposition in the Brookhaven chamber was achieved by exposing the Au(111) surface to $\sim 1\times 10^{-7}$ mbar of $Mo(CO)_6$ at 500 K, followed by annealing in a vacuum at 600 K for 5 min. The $Mo(CO)_6$ was kept in a glass tube at room temperature and briefly pumped before each dose. This design of the doser could induce part of the $Mo(CO)_6$ to decompose while dosing. The exposures of $Mo(CO)_6$ were measured by an uncorrected ion gauge; part of the ion gauge reading could be attributed to CO, which could lead to large apparent exposures to get small coverages. STM images of the dosed surfaces were acquired at room temperature using a W tip. Molybdenum surface coverages on terraces were estimated from STM images and expressed as a fraction (%) of the surface area covered by Mo. For reasons discussed later, this estimate does not account for the increase in cluster heights with increasing coverage. At Harvard, the same dosing procedure was used, with the exception that the dosed surface was briefly heated to 600 K. A Pt(10%)−Ir tip was used for STM data acquisition.

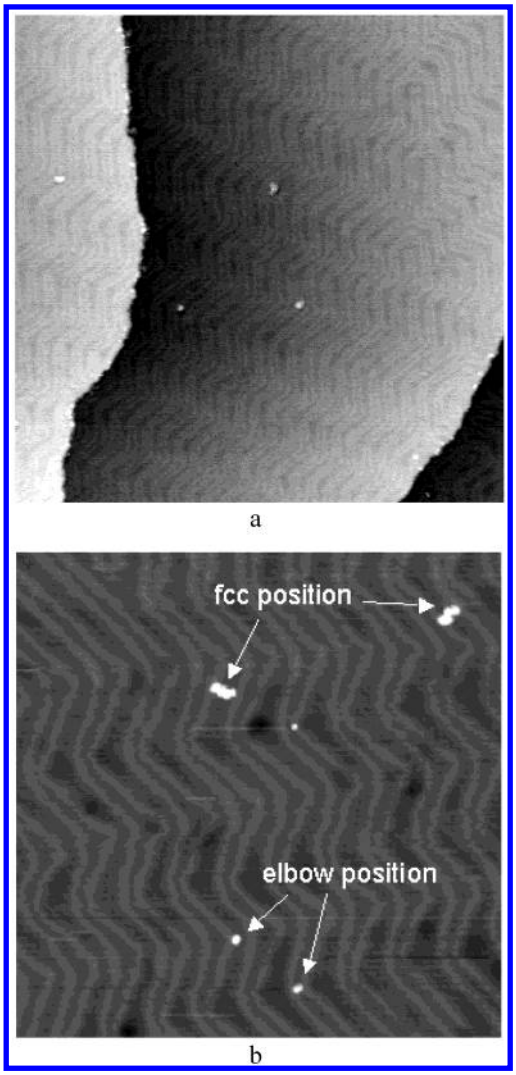

Figure 1. STM images of 0.1% Mo coverage (% of surface area covered by clusters and islands) on Au(111) obtained by exposure to 16 L of $Mo(CO)_6$ at 500 K and annealed to 600 K. The images were taken at room temperature. Image sizes: (a) (200 × 200) nm^2; (b) (75 × 75) nm^2.

Results and Discussion

Metallic Mo clusters are deposited by decomposition of $Mo(CO)_6$ on the Au(111) herringbone surface at 500 K (Figures 1−3). The coverages of Mo deposited from integrated exposures of 16, 32, and 60 L of $Mo(CO)_6$ at $\sim 1\times 10^{-7}$ mbar are 0.1, 1.4,

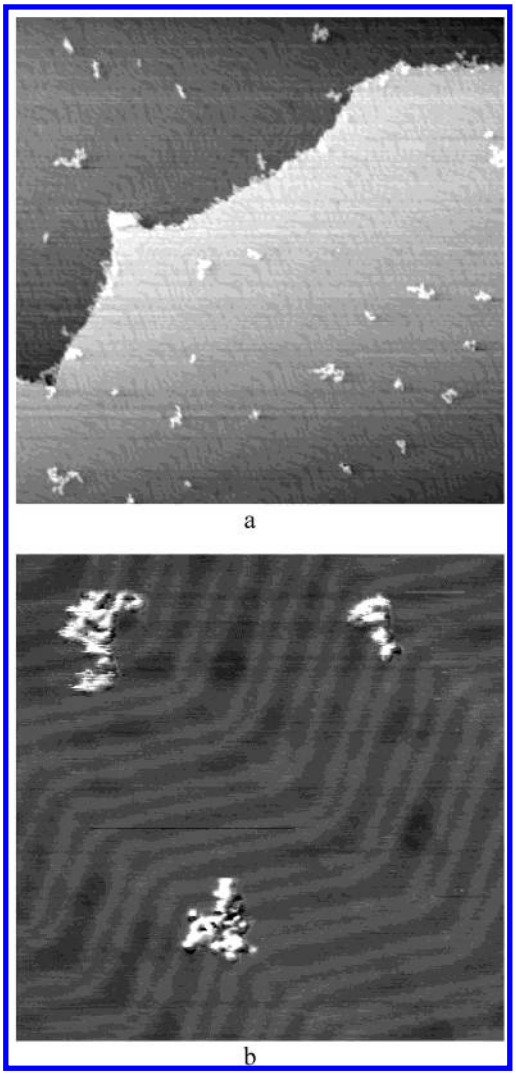

Figure 2. STM images of 1.4% Mo coverage on Au(111) obtained by exposure to 32 L of $Mo(CO)_6$. Image sizes: (a) (280 × 280) nm^2; (b) (60 × 60) nm^2.

and 5.5%, respectively. These results are consistent with our previous photoemission study which showed that $Mo(CO)_6$ decomposed on Au(111) above 400 K.[15] No C or O was detected by photoemission or Auger electron spectroscopy for low coverages (∼0.15 ML) of Mo deposited from $Mo(CO)_6$ on the Au(111) at 500 K.

The $Mo(CO)_6$ decomposition on metal surfaces is a thermally activated process: a $Mo(CO)_6$ multilayer adsorbed at low temperatures primarily desorbs with ∼2% of the first layer decomposing via decarbonylation.[15] It is unlikely that $Mo(CO)_6$ decomposition is promoted by charge transfer between the substrate and the adsorbed carbonyl molecules,[16b,38] because there is a low probability for electron transfer given the ∼2 eV energy difference between the Fermi level of Au and the lowest $Mo(CO)_6$ antibonding state ($4d^*(^1T_{1g})$) (using 5.3 eV as the work function of Au(111)).[39]

The rate of $Mo(CO)_6$ dissociation is increased by heating the gold surface to 500 K. At this temperature the energy imparted to the molecule is sufficient for dissociation of the first CO−Mo−$(CO)_5$ bond which has a bond energy of ∼40 kcal/mol.[16] Once one Mo−CO bond is broken, the carbonyl fragments can bond to the surface and to each other to form clusters. The remaining CO molecules can be stripped off thermally.[12] However, at 500 K some CO could be adsorbed or re-adsorbed on the Mo clusters and affect the growth of Mo.[16b] For comparison, temperatures around 600 K are needed to desorb CO from Mo(110) at low coverages.[40]

In initial stages of Mo deposition, Mo clusters, imaged as bright dots, are observed both on terraces and at steps (Figure 1). Most clusters on the terraces are located at elbows of the herringbone reconstruction; however, some clusters juxtapose (i.e., aggregate without coalescence) within the fcc stacking regions to form cluster islands. In the rest of the paper we will use the "island" term to mean an island composed of individual Mo clusters. Clusters and islands that grow at step edges are located at both the upper and the lower steps as is evident from the brightness contrast. As the Mo coverage increases, the number of Mo clusters and the size of the aggregated cluster islands increase (Figure 2). At the Mo coverage of 1.4%, nearly all clusters are incorporated into islands. The clusters within these islands do not coalesce; rather, they are ramified with the centers of islands located mostly at elbows. Increasing the coverage further to 5.5% leads to larger aggregates (Figure 3). Even at these higher coverages, the STM images show clearly that the clusters do *not* coalesce. Instead, the clusters remain ramified with preferred orientations along the fcc troughs and the domain boundary directions. Decoration of both the upper and lower step edges with cluster islands persists at these higher coverages.

It is worth mentioning that the deposition of Mo on Au did not alter the superstructure of the Au surface. Irregularities of the herringbone pattern (i.e., uniaxial domain boundaries) seen in Figure 3b are also typical of a clean surface and we did not observe any Mo-induced changes for coverages investigated in this work.

Figure 3c shows the cluster size distribution ranging from 1 to 3.5 nm with a maximum at 1.8 nm. As the cluster diameter vs height ratio is constant for a given bias voltage, the upper limit of cluster sizes was estimated by measuring the apparent diameters of the clusters from their STM images. The absolute height of the clusters in this system cannot be quantitatively determined because it is bias voltage dependent (Figure 4). While the topographic height difference between the herringbone stripes and hcp area is 0.01 nm and quite independent of bias voltage in the range of −0.4 V to −2 V, the apparent height of the Mo cluster increases 5-fold (from 0.06 to 0.3 nm) over the same voltage range. This effect may be caused by a band gap near the Fermi level of the Mo cluster due to its small size.

Over the range of Mo coverages studied, the sizes of clusters within the islands do not increase noticeably with increasing coverage. The narrow and constant size distribution suggests that the growth of Mo clusters is self-limiting. A possible reason for this behavior is the presence of CO, which could have size-dependent adsorption behavior on Mo clusters and influence their growth.

Although the size of the clusters is constant, the number of clusters per island does increase with increasing coverage. Figure 3d shows the island size distribution in terms of the number of clusters with an average size of 1.8 nm. For comparison, a Poisson distribution of the island size is also shown in Figure 3d. It was calculated by assuming that the nucleation event has an identical probability. The maximum of Poisson distribution was chosen at 14 clusters per island, to be close to the experimental island size distribution. The measured Mo island size distribution is very broad with a long tail, ranging from 1 to approximately 90 clusters. Significant differences between the measured and Poisson distributions of the Mo islands therefore imply that larger islands have clearly higher probability of capturing mobile Mo clusters.

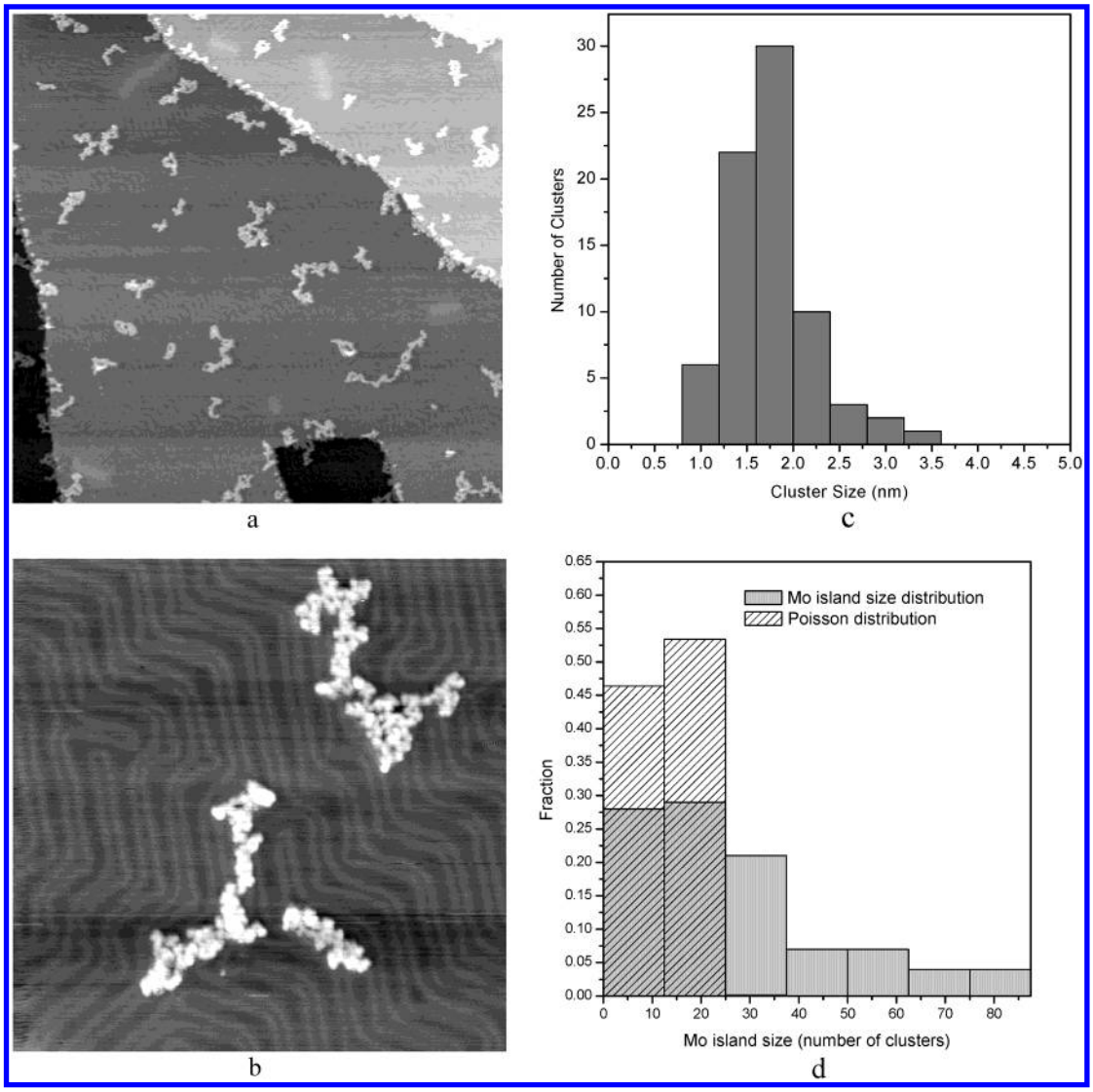

Figure 3. STM images of 5.5% Mo coverage on Au(111) obtained by exposure to 60 L of $Mo(CO)_6$. Image sizes: (a) (485 × 485) nm^2; (b) (54 × 54) nm^2; (c) cluster size distribution; (d) islands size distribution in terms of cluster number in each island.

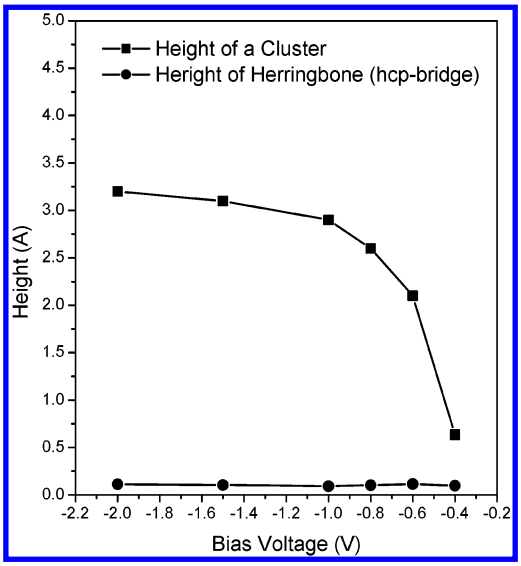

Figure 4. The apparent height of a cluster and the height of the herringbone stripes vs the hcp trough as a function of the tip bias.

Besenbacher et al.[28] studied the growth of Mo on Au(111) by PVD of Mo atoms. They found that Mo nucleated at *all* elbows and at step edges. Compact Mo clusters formed a well-ordered array reflecting the pattern in the surface arising from the reconstruction. Mo, the element with a higher surface free energy than Au and higher heat of sublimation, follows the prediction of preferential nucleation at elbows due to site selective place exchange as proposed by Meyer et al.[41]

For the Mo/Au(111) system, the elbows are the nucleation sites and their density on a reconstructed Au surface is about 6 × $10^{11}cm^{-2}$. If the number of the islands is controlled by the number of the available nucleation sites, then these two values should be comparable. In the case of CVD growth of Mo on Au(111), for the apparent coverages ranging from 0.1 to 5%, the density of the cluster islands is approximately constant (∼5 × 10^{10} cm^{-2}) and 1 order of magnitude smaller than the density of elbows (see Figure 5). This result implies that the Mo clusters formed in the CVD process do not interact strongly with the elbow nucleation sites as in the PVD process.

The evolution of the Mo islands morphology with increasing coverage suggests that the islands are formed by diffusion-limited aggregation (DLA)[42] of the clusters. In the original computer simulation, randomly ramified islands are formed as diffusing particles hit and stick irreversibly to a growing island. Experimentally, a growth of dendritic islands was observed in bimetallic systems,[43] and anisotropy of either substrate or the

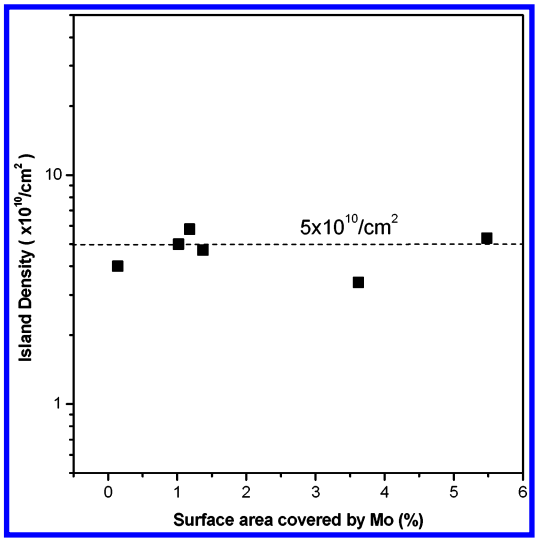

Figure 5. Area density of Mo clusters and islands as a function of coverage expressed as % surface area covered.

aggregating particles is crucial for dendritic growth.[44] Metal islands can be characterized by fractal dimension d_f determined from the $A^{1/2}$ vs P^{1/d_f} plot, where A is the area and P is the perimeter of the island. Both randomly ramified and dendritic islands have a fractal dimension d_f close to 1.7 and its value may provide information about the growth mechanism; e.g., if there is an energy barrier for the aggregation, the clusters will not stick immediately. This will lead to a reaction-limited cluster aggregation and formation of more compact, polydispersed islands with $d_f = 2.1$ as shown in studies of phase transition kinetics of colloids.[45,46] The ramified Mo islands studied in this work have $d_f = 1.7$ and this value suggests that the underlying growth mechanism can be described by DLA and the Mo clusters are the mobile aggregating particles.

It is interesting that the ramified islands, formed by clusters aggregating in the CVD process, have island morphology similar to those observed previously in mass-selected cluster deposition experiments. In the latter case, the motion of clusters on surfaces and the interaction among clusters are used to explain the island morphology. Yoon et al.[47] explained the dependence of island morphology on Sb cluster size by invoking a critical cluster size, R_0, such that island shapes were compact for $R < R_0$ and ramified for $R > R_0$. They assumed that there was a competition between cluster aggregation and coalescence dictated by the time interval between successive arrivals of clusters. Perez et al.[48] used the Arrhenius law to fit the temperature-dependent diffusion coefficient of Sb_{2300} and Au_{250} clusters by applying the predictions of the deposition−diffusion−aggregation model to the observed island morphologies, and found large preexponential factors. They pointed out the diffusion mechanisms of these clusters must involve rotational movement of the cluster. This could explain why two clusters become immobile when they become attached, which is the mechanism for the growth of a ramified island. Jensen[49] and Binns[50] in their recent review articles analyzed the growth of nanostructures by direct cluster deposition and several conclusions are applicable for CVD growth discussed in this work.

The ramified island morphology observed in our study clearly indicates that the Mo clusters formed from $Mo(CO)_6$ are mobile on the surface during nucleation and growth. Previous work clearly indicates that cluster mobility determines the types of islands formed. In turn, cluster diffusion reflects the strength of cluster−substrate interaction. If the cluster−substrate interaction is strong when compared to kT, the clusters are relatively immobile. A weaker interaction leads to higher mobility of clusters that is reflected in a low density of islands. The island morphology, on the other hand, reflects cluster−cluster interaction since a cluster that arrives at an island can either coalesce or remain separate to form a ramified island. The coalescence of clusters is driven by thermodynamics as the system is trying to minimize the surface free energy. The ramification is a kinetic effect because the clusters' arrival rate is faster than their incorporation, thus preventing the free energy minimization. Accordingly, the ramified cluster island structure in the CVD growth of Mo on Au(111) implies that the Mo clusters form and move around before they anchor on the surface.

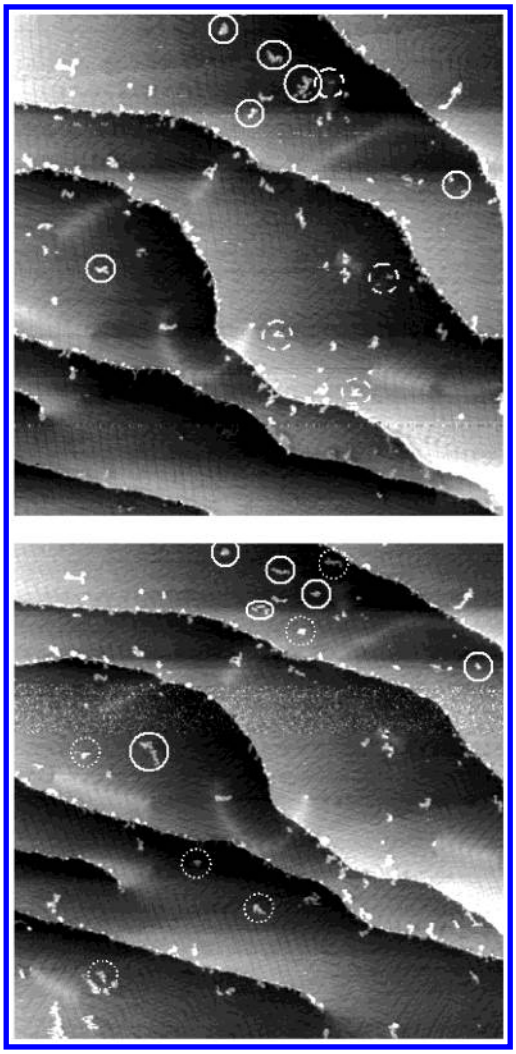

Figure 6. Two consecutive STM images with highlighted changes in surface morphology taken 7 min apart: full circle, changed; dotted circle, disappeared; dashed circle, new feature. The sample was not annealed after being exposed to $Mo(CO)_6$ at 500 K. Image sizes: (400 × 400) nm^2

The mobility of Mo clusters is demonstrated in two sequential STM images (Figure 6). The sample was prepared without annealing after dosing $Mo(CO)_6$ on Au(111) at 500 K. Approximately 15% of the islands on terraces either change in size or move to another location on a time scale of minutes at room temperature. We did not observe analogous cluster mobility if the sample was annealed to 600 K after deposition, indicating that annealing reduces the mobility of the clusters. Therefore, the observed mobility can be related to the presence of the residual CO on the Mo clusters.[16b] As there is a large CO pressure during the CVD growth, the Mo clusters are probably covered by CO molecules. The adsorbed CO may reduce both

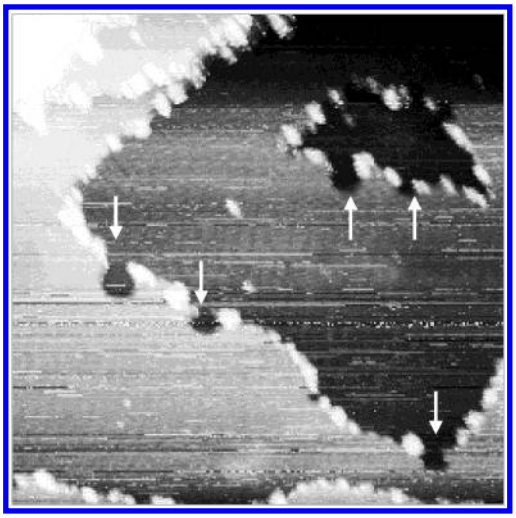

Figure 7. Holes and kinks (indicated by arrows) formed at the step edges of Au(111) after depositing Mo at 500 K from $Mo(CO)_6$ at lower dosing pressure. Image size: (200 × 200) nm^2.

Mo−Mo and Mo−Au interactions[16b] with the net result of Mo clusters weakly bonded to the Au surface. Indeed, there is precedence for enhanced mobility of Pt induced by adsorbed CO.[51] The limited decoration of elbows also indicates the weakening of the Mo−Au interaction. In the PVD process, Mo clusters are strongly bonded and energy dissipation into gold substrate is facile. With clusters poorly coupled to the surface in the CVD case, the attachment of additional Mo to the clusters may lead to kinetic energy gain from the Mo−Mo bond formation. We are currently investigating the underlying reasons for the mobility of the clusters formed during deposition at 500 K.[52,53]

Another apparent difference in the $Mo(CO)_6$ CVD of Mo from the PVD is that Mo clusters grow at both upper and lower step edges as seen in Figures 2a and 3a. In PVD of metal atoms on metal substrates, clusters appear to grow only at the lower step edges.[54] There is an asymmetry in the surface potential energy of a metal adatom or cluster on a substrate near step edges: a trapping well at the lower terrace side and a repulsive barrier at the upper one. Therefore, metal atoms or clusters are usually trapped at the lower terrace side of step edges and grow from there in the so-called step flow mode. The growth of Mo clusters both at the top and bottom of step edges indicates that there is a potential well associated with the step that leads to the trapping of growing clusters. This finding may be the result of the presence of the dipole field at step edges that causes preferential adsorption of Mo-containing species at the upper step edges.[55]

We have direct evidence (Figure 7) for removal of Au at steps during growth of Mo clusters deposited from $Mo(CO)_6$. The removal of Au at the step edge is manifested by the development of holes and kinks at steps of the Au surface during deposition of Mo when using lower dosing pressure of $Mo(CO)_6$. Under these conditions Mo clusters grow predominantly at Au steps. Holes and kinks at Au step edges are *not* present on clean Au(111) or on CO-dosed Au(111) using the same dosing parameters for $Mo(CO)_6$ (data not shown). These data suggest that while CO may facilitate the transport of atoms and/or clusters on the Au surface, CO alone cannot be responsible for the removal of Au atoms from the steps. One plausible explanation is that the Au atoms removed are incorporated into the Mo clusters. Another possibility is the step pinning by the Mo clusters and consequential alternation of the step flow. Alternatively, the step atom removal can be linked to the vacancy exchange between the surface and the bulk. The surfaces are known to be good sink of bulk vacancies[56] and the step movement can be affected by the presence of the Mo clusters at the step edges, thus leading to roughening of the steps.

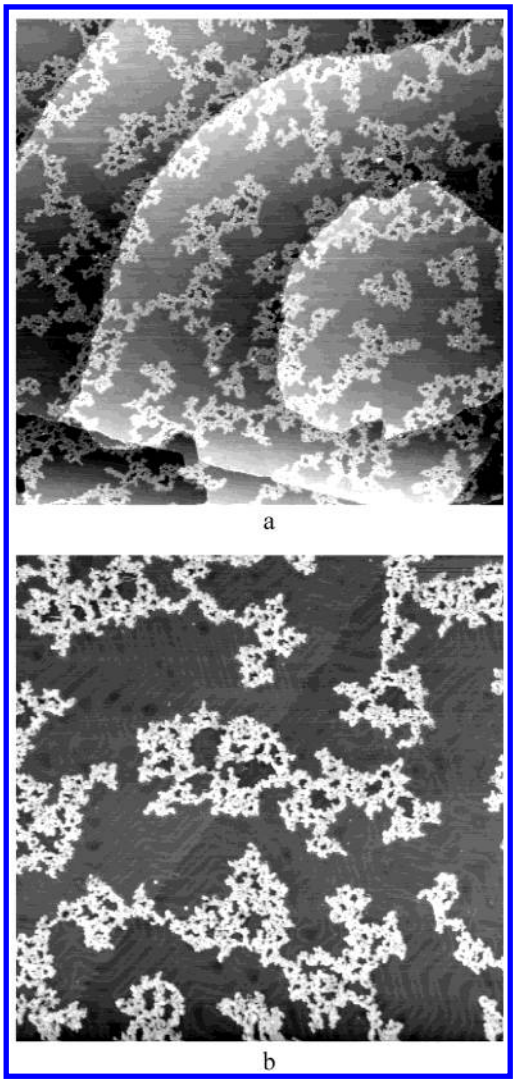

Figure 8. STM images of a MoO_3-covered Au(111) sample acquired after NO_2 oxidation of the sample shown in Figure 3. Image sizes: (a) (400 × 400) nm^2; (b) (200 × 200) nm^2.

Considering the large differences of surface free energy of Au and Mo[57] one may assume that when all CO ligands detach from a Mo center in $Mo(CO)_6$, a place exchange of the substrate gold atoms by Mo atoms may occur for decreasing the surface free energy of the system. The molybdenum−gold place exchange is predicted by first-principle density functional calculations.[51,53,58] A consequence of this place exchange mechanism is that Mo clusters would be embedded in the Au substrate.[53] As Au and Mo are bulk immiscible, Au atoms ejected from the substrate or detached from the steps are likely to cap the Mo cluster. The absence of reactivity toward CO, S_2, thiophene, O_2, and C_2H_4[15,59] for clusters formed by $Mo(CO)_6$ decomposition on Au(111) is consistent with the capping of these clusters by Au atoms. The most conclusive evidence in support of this is found in oxidation reactions.[59] Molecular oxygen shows little reactivity, but reaction with NO_2 leads to formation of molybdenum oxides with a single Mo 3d doublet and O 1s core levels characteristic of MoO_3. As gold does not react with O_2, Mo clusters capped with Au should also be inert to O_2, in contrast to the behavior with atomic oxygen produced by the decomposition of NO_2.

Oxidation of Mo clusters and islands with NO_2 leads to the formation of 2D MoO_3 structures, details of which will be described in a separate paper.[60] Figure 8 shows STM images of MoO_3 structures obtained after NO_2 oxidation at 500 K of the 5.5% Mo-covered surface in Figure 3. A substantial increase in the apparent adlayer coverage of the MoO_3-covered surface is observed, as compared to the Mo-covered surface. Furthermore, the PES intensity of the Mo 3d core levels of the MoO_3-covered surface was about 2.5 times higher than that of the metallic Mo-covered surface, although both spectra were measured from the same Mo/Au sample before and after oxidation.[59] The observed intensity increase was ascribed to a morphology change induced by the oxidation. MoO_3 is a layered molecular crystal with layers held weakly by van der Waals interactions. We propose that the MoO_3 forms 2D islands with the (010) facet parallel to the Au(111) surface. If the metallic Mo clusters were 2D crystallites, the conversion from Mo(100) or Mo(110) clusters to the MoO_3(010) would result in an increase of the adlayer coverage by a factor of 1.7 or 2.4, respectively. From STM images, however, the oxidation brings an increase of the coverage by a factor of 6. We therefore conclude that the metallic Mo clusters deposited on Au(111) from $Mo(CO)_6$ are 3D clusters of about 2−3 layers of Mo thick either above the surface or in part embedded in the gold substrate.

Conclusion

By monitoring the morphology change at different Mo coverages with STM, the growth of Mo on Au(111) using $Mo(CO)_6$ as a precursor is summarized in the following scheme:

$$y\mathrm{Mo(CO)_6} \rightarrow y\mathrm{Mo(CO)_x} \rightarrow \mathrm{Mo_y(CO)_x} \rightarrow z\{\mathrm{Mo_y(CO)_x}\} \rightarrow z\{\mathrm{Mo_y}\}$$

Adsorption of carbonyl on a gold surface at elevated temperatures is followed by decarbonylation. Deposited carbonyl fragments nucleate to form Mo nanoclusters $\{Mo_y\}$. The clusters formed in the process are mobile on the surface, leading to formation of ramified islands ($z\{Mo_y\}$).

There are important differences with respect to PVD of Mo atoms on Au(111). In the CVD process, $Mo(CO)_6$ molecules decompose on a Au(111) surface at elevated temperature and form Mo 3D nanoclusters. On terraces, the clusters start to decorate elbow sites. However, with the increase of Mo coverage, more clusters are formed and aggregate to develop ramified islands rather than being trapped uniformly at other elbows. The Mo clusters gain kinetic energy during their formation, decreasing the probability of their trapping at the elbow positions. Ramified islands are formed when clusters stop their motions once they meet others. At step edges, the ramified islands grow at both upper and lower terrace sides, in contrast to the PVD growth at the lower step edge. The former can be attributed to the finite residence of CO on the upper step edges, which modifies the surface potential of Mo on Au step edges.

Acknowledgment. A part of this research carried out at Brookhaven National Laboratory was supported under Contract DE -AC02-98CH10086 with the U.S. Department of Energy, Division of Chemical Sciences. The research at Harvard was supported by the National Science Foundation through the Nanoscale Science and Engineering Center at Harvard, No. PHY-011-7795. A.S.Y.C. also gratefully acknowledges a Materials Research Science and Engineering Center Postdoctoral Fellowship funded by NSF Grant DMR-98-09363.

References and Notes

(1) Psaro, R.; Recchia, S. *Catal. Today* **1998**, *41*, 139.
(2) Alexeev, O.; Gates, B. C. *Top. Catal.* **2000**, *10*, 273.
(3) Huh, S. H.; Oh, S. J.; Kim, Y. N.; Lee, G. H. *Rev. Sci. Instrum.* **1999**, *70*, 4366.
(4) Commereuc, D.; Chauvin, Y.; Hugues, F.; Basset, J. M.; Olivier, D. *Chem. Commun.* **1980**, 154.
(5) Hugues, F.; Besson, V.; Basset, J. M. *Chem. Commun.* **1980**, 719.
(6) Hugues, F.; Dalmon, J. A.; Bussiere, P.; Smith, A. K.; Basset, J. M.; Olivier, D. *J. Phys. Chem.* **1982**, *86*, 5136.
(7) Bielawa, H.; Hinrichsen, O.; Birkner, A.; Muhler, M. *Angew. Chem., Int. Ed.* **2001**, *40*, 1061.
(8) Close, M. R.; Petersen, J. L.; Kugler, E. L. *Inorg. Chem.* **1999**, *38*, 1535.
(9) de Bont, P. W.; Vissenberg, M. J.; de Beer, V. H. J.; van Veen, J. A. R.; van Santen, R. A.; van der Kraan, A. M. *Appl. Catal. A* **2000**, *202*, 99.
(10) Green, M. L.; Levy, R. A. *J. Metals* **1985**, 63.
(11) Cho, C. C.; Bernasek, S. L. *J. Appl. Phys.* **1989**, *65*, 3035.
(12) Xu, M.; Zaera, F. *J. Vac. Sci. Technol. A* **1996**, *14*, 415.
(13) Argo, A. M.; Odzak, J. F.; Lai, F. S.; Gates, B. C. *Nature* **2002**, *415*, 623.
(14) Malik, I. J.; Hrbek, J. *J. Vac. Sci. Technol.* ***A*** **1991**, *9*, 1737.
(15) Rodriguez, J. A.; Dvorak, J.; Jirsak, T.; Hrbek, J. *Surf. Sci.* **2001**, *490*, 315.
(16) (a) Lewis, K. E.; Golden, D. M.; Smith, G. P. *J. Am. Chem. Soc.* **1984**, *106*, 3905. (b) Liu, P.; Rodriguez, J. A.; Muckerman, J. T.; Hrbek, J. *Surf. Sci.*, in press.
(17) Tøpsoe, H.; Clausen, B. S.; Massoth, F. E. *Hydrotreating Catalysis*; Springer-Verlag: New York, 1996.
(18) Startsev, A. N. *Catal. Rev. Sci. Eng.* **1995**, *37*, 353.
(19) Chianelli, R. R.; Daage, M.; Ledoux, M. *Adv. Catal.* **1994**, *40*, 177.
(20) Dellmon, B. *Bull. Soc. Chim. Belg.* **1995**, *104*, 173.
(21) Barth, J. V.; Brune, H.; Ertl, G.; Behm, R. J. *Phys. Rev. B* **1990**, *42*, 9307.
(22) Chambliss, D. D.; Wilson, R. J.; Chiang, S. *Phys. Rev. Lett.* **1991**, *66*, 1721.
(23) Voigtländer, B.; Meyer, G.; Amer, N. M. *Surf. Sci.* **1991**, *255*, L529.
(24) Voigtländer, B.; Meyer, G.; Amer, N. M. *Phys. Rev. B* **1991**, *44*, 10354.
(25) Padovani, S.; Chado, I.; Scheuer, F.; Bucher, J. P. *Phys. Rev. B* **1999**, *59*, 11887.
(26) Padovani, S.; Chado, I.; Scheuer, F.; Bucher, J. P. *Phys. Rev. B* **2000**, *61*, 72.
(27) Chado, I.; Scheurer, F.; Bucher, J. P. *Phys. Rev. B* **2001**, *64*, 094410.
(28) Helveg, S.; Lauritsen, J. V.; Lægsgaard, E.; Stensgaard, I.; Nørskov, J. K.; Clausen, B. S.; Topsøe, H.; Besenbacher, F. *Phys. Rev. Lett.* **2000**, *84*, 951.
(29) Wang, Z.; Moskovits, M. *J. Appl. Phys.* **1992**, *71*, 5401.
(30) Dovek, M. M.; Lang, C. A.; Nogami, J.; Quate, C. F. *Phys. Rev. B* **1989**, *40*, 11973.
(31) Chambliss, D. D.; Wilson, R. J. *J. Vac. Sci. Technol. B* **1991**, *9*, 928.
(32) Brune, H.; Giovannini, M.; Bromann, K.; Kern, K. *Nature* **1998**, *394*, 451.
(33) Hrbek, J.; Hwang, R. Q. *Curr. Opin. Solid State Mater. Sci.* **2001**, *5*, 67.
(34) Fischer, B.; Brune, H.; Barth, J. V.; Fricke, A.; Kern, K. *Phys. Rev. Lett.* **1999**, *82*, 1732.
(35) Brune, H. *Surf. Sci. Rep.* **1998**, *31*, 121.
(36) Strbac, S.; Magnussen, O. M.; Behm, R. J. *Phys. Rev. Lett.* **1999**, *83*, 3246.
(37) Clark, P. G., Jr.; Friend, C. M. *J. Chem. Phys.* **1999**, *111*, 6991.
(38) Ying, Z. C.; Ho, W. *J. Chem. Phys.* **1991**, *94*, 5701.
(39) Skriver, H. L.; Rosengaard, N. M. *Phys. Rev. B* **1992**, *46*, 7157.
(40) Chen, J. G.; Colaianni M. L.; Weinberg W. H.; Yates, J. T., Jr. *Chem. Phys. Lett.* **1991**, *177*, 113.
(41) Meyer, J. A.; Baikie, I. D.; Kopatzki, E.; Behm, R. J. *Surf. Sci.* **1996**, *365*, L647.
(42) Witten, T. A., Jr.; Sanders, L. M. *Phys. Rev. Lett.* **1981**, *47*, 1400.
(43) Hwang, R. Q.; Schröder, J.; Günther, C.; Behm, R. J. *Phys. Rev. Lett.* **1991**, *67*, 3279.
(44) Brune, H.; Roder, H.; Bromann, K.; Kern, K.; Jacobsen, J.; Stolze, P.; Jacobsen, K.; Norskov, J. *Surf. Sci.* **1996**, *349*, L115.
(45) Weitz, D. A.; Huang, J. S.; Lin, M. Y.; Sung. J. *Phys. Rev. Lett.* **1985**, *54*, 1416.
(46) Anderson, V. J.; Lekkerkerker, H. N. W. *Nature* **2002**, *416*, 811.
(47) Yoon, B.; Akulin, V. M.; Cahuzac, Ph.; Carlier, F.; de Frutos, M.; Masson, M.; Mory, C.; Colliex, C.; Bréchignac, C. *Surf. Sci.* **1999**, *443*, 76.

(48) Perez, A.; Melinon, P.; Dupuis, V.; Jensen, P.; Prevel, B.; Tuaillon, J.; Bardotti, L.; Martet, C.; Treilleux, M.; Broyer, M.; Pellarin, M.; Vaille, J. L.; Palpant, B.; Lerme, J. *J. Phys. D: Appl. Phys*. **1997**, *30*, 709.
(49) Jensen, P. *Rev. Mod. Phys.* **1999**, *71*, 1695.
(50) Binns, C. *Surf. Sci. Rep.* **2001**, *44*, 1.
(51) Kalff, M.; Comsa, G.; Michely, T. *Phys. Rev. Lett*. **1998**, *81*, 1255.
(52) Chan, Ally, S. Y.; Friend, C. M. To be published.
(53) Liu, P.; Rodriguez, J. A; Muckerman, J. T.; Hrbek, J. *Phys. Rev. B*, submitted.
(54) Günther, C.; Günther, S.; Kopatzki, E.; Hwang, R. Q.; Schröder, J.; Vrijmoeth, J.; Behm, R. J. *Ber. Bunsen-Ges. Phys. Chem.* **1993**, *97*, 522.
(55) Pascual, J. I.; Jackiw, J. J.; Kelly, K. F.; Conard, H.; Rust, H.-P.; Weiss, P. S. *Phys. Rev. B* **2000**, *62*, 12632.
(56) McCarty, K. F.; Nobel, J. A.; Bartelt, N. C. *Nature* **2001**, *412*, 622.
(57) Mezey L. Z.; Giber, J. *Jpn. J. Appl. Phys.* **1982**, *21*, 1569.
(58) Ruban, A. V.; Skriver, H. L.; Nørskov, J. K. *Phys. Rev. B* **1999**, *59*, 15990.
(59) Chang, Z.; Song, Z.; Liu, G.; Rodriguez, J. A.; Hrbek, J. *Surf. Sci.* **2002**, *512*, L353.
(60) Song, Z., et al. To be published.